Available online at www.sciencedirect.com
SCIENCE DIRECT®
Journal of Process Control 16 (2006) 27–35
JOURNAL OF PROCESS CONTROL
www.elsevier.com/locate/jprocont

Multi-objective model-based control for an automotive catalyst

Kenneth R. Muske [a,*], James C. Peyton Jones [b]

[a] Department of Chemical Engineering, Villanova University, Villanova, PA 19085, USA
[b] Department of Electrical and Computer Engineering, Villanova University, Villanova, PA 19085, USA

Received 1 December 2004; received in revised form 23 March 2005; accepted 29 April 2005

Abstract

A model-based feedforward/feedback air fuel ratio controller that optimizes the oxygen storage capacity of the three-way catalyst in automotive emission control systems is presented. This work incorporates a simplified dynamic catalyst model that describes the physical behavior of oxygen chemisorption and reversible deactivation in the catalyst system. A novel aspect of this work is the use of the oxygen storage capability of the catalyst not only to minimize vehicle emissions but also to optimize engine performance and fuel economy during transient engine demand. The feedback/feedforward controller is a nonlinear model predictive controller that incorporates catalyst, engine air fuel ratio controller, and fuel system models to determine the optimal air fuel ratio target trajectory. Feedback is provided by a nonlinear moving horizon estimation strategy for the determination of the oxygen storage level of the catalyst based on air fuel ratio sensors.

Keywords: Automotive three-way catalyst; Automotive catalyst control

1. Introduction

The use of three-way catalysts in exhaust after-treatment systems is essential in reducing tail-pipe emissions to the levels demanded by environmental legislation. Although improvements in catalyst formulation and substrate design to reduce automotive emissions are on-going, there is considerable potential for reduction from advanced control of the catalyst operation [1]. As environmental legislation continues to impose increasingly stringent tail-pipe emission regulations, realizing the potential of advanced catalyst control will become more important for regulatory compliance.

Model-based techniques offer an attractive advanced control methodology for automotive catalyst systems. A critical aspect of any model-based approach, however, is the ability of the model to predict the dynamic behavior of the catalyst system and the ability to estimate the current state of the system model from available measurements. This work incorporates a simplified dynamic catalyst model that closely captures the dynamic behavior of oxygen chemisorption and reversible deactivation. A moving horizon estimation strategy for the catalyst oxygen storage level based on pre- and post-catalyst wide range or universal exhaust gas oxygen (UEGO) sensor measurements is proposed in this work. This estimator provides accurate dynamic estimates while the state is unobservable and reliable model updates when the state becomes observable.

2. Catalyst operation

Key to the operation of three-way catalyst systems is the ability to store and release oxygen resulting from chemisorption/desorption with the cerium oxides contained in the catalyst. Under rich (excess fuel) engine operation, the catalyst oxidizes the hydrocarbons and

* Corresponding author. Tel.: +1 610 519 6195; fax: +1 610 519 7354.
E-mail address: kenneth.muske@villanova.edu (K.R. Muske).

0959-1524/$ - see front matter © 2005 Elsevier Ltd. All rights reserved.
doi:10.1016/j.jprocont.2005.04.008

carbon monoxide present in the incoming exhaust gas by releasing previously stored oxygen. This oxygen release maintains stoichiometric combustion with commensurately low levels of hydrocarbon and carbon monoxide emissions. Because of the finite storage capacity of the catalyst, however, this process cannot continue indefinitely. When the oxygen release rate of the depleted catalyst can no longer satisfy the demand, the post-catalyst air fuel ratio will decrease below stoichiometric and hydrocarbon breakthrough will eventually occur. A typical catalyst control system will therefore attempt to switch to lean (excess air) engine operation before this breakthrough condition is encountered. Under lean engine operation, the excess oxygen in the exhaust gas is now adsorbed onto the catalyst resulting in near-stoichiometric post-catalyst conditions and low tail-pipe emissions. As the oxygen storage capacity of the catalyst approaches its saturation condition, however, the post-catalyst oxygen concentration increases above stoichiometric and breakthrough of nitrogen oxides will eventually occur. A typical catalyst control system will then attempt to switch back to rich engine operation before lean breakthrough. By cycling the engine operation in this way, the oxygen storage capacity of the catalyst can be used as a buffer against breakthrough by compensating for transient oxygen excess or deficiency.

This dynamic behavior is clearly shown in Fig. 1 where the post-catalyst air fuel ratio remains essentially at stoichiometric (≈14.5) for several seconds after the pre-catalyst air fuel ratio makes a lean to rich step transition. Air fuel ratio is defined as the ratio of the air mass flow rate to the fuel mass flow rate. When the oxygen release rate of the catalyst can no longer satisfy the exhaust gas demand, the post-catalyst air fuel ratio begins to become rich until it eventually matches the pre-catalyst air fuel ratio. The separation between the pre- and post-catalyst sensor measurements present between 20 and 70 s is due to sensor distortion in the post-catalyst air fuel ratio sensor as discussed in the sequel. Oxygen storage on the catalyst is clearly shown after the pre-catalyst air fuel ratio rich-to-lean step change made at approximately 70 s.

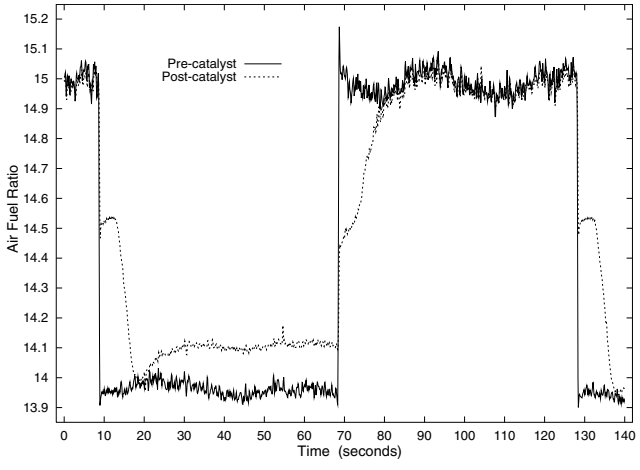

Fig. 1. Pre- and post-catalyst air fuel ratio transitions.

3. Catalyst system model

The catalyst system model used in the model-based controller is described in this section. This model consists of a combination of component models representing the catalyst oxygen storage, post-catalyst sensor distortion, engine air fuel ratio controller, and fuel system. These component models are discretized and integrated into a single model of the system. A moving horizon estimator is employed to determine the current state of the system model for the controller.

3.1. Catalyst oxygen storage model

Various models have been proposed for the real-time characterization of the dynamic oxygen storage, or equivalently of the rate oxygen storage and release. In the simplest case, used implicitly or explicitly in many current systems, the catalyst is represented as a limited integrator oxygen store, where the rate of storage or release is proportional to the relative oxygen excess or deficiency in the pre-catalyst exhaust gas. A significant model improvement is described in [2], with later refinements in [3], where the model structure is preserved, but rates of oxygen storage and release are considered to be nonlinear functions of the amount of oxygen stored on the catalyst. These functions switch according to whether the catalyst is being oxidized or reduced by the pre-catalyst exhaust gas. The catalyst oxygen storage in this work is represented by the following nonlinear integrating model [4]

$$\dot{\phi} = K_\lambda \dot{m}_\mathrm{f}(\Delta\lambda^{\triangleleft} - \mathscr{N}(\phi)), \tag{1}$$

where ϕ is the oxygen storage state of the catalyst, $\dot{m}_\mathrm{f}$ is the fuel mass flow rate to the engine, $\mathscr{N}(\phi)$ is the equilibrium oxygen storage capacity of the catalyst, and $\Delta\lambda^{\triangleleft}$ is the pre-catalyst relative air fuel ratio deviation from stoichiometric with $\Delta\lambda$ defined as

$$\Delta\lambda = \lambda - 1, \quad \lambda = \frac{1}{K_\lambda}\frac{\dot{m}_{\mathrm{O}_2}}{\dot{m}_\mathrm{f}}, \tag{2}$$

where $\lambda = 1$ represents a stoichiometric air fuel ratio, $\dot{m}_{\mathrm{O}_2}$ is the oxygen mass flow rate to the engine, and K_λ is the stoichiometric air fuel ratio times the oxygen mass fraction of air. In this model, the oxygen storage and release rates depend on the difference between the forcing function $\Delta\lambda^{\triangleleft}$, which promotes adsorption under lean air fuel ratio conditions and desorption under rich air fuel

ratio conditions, and the equilibrium catalyst oxygen storage $\mathcal{N}(\phi)$.

This model describes stored oxygen relative to the equilibrium level when the pre-catalyst exhaust gas is stoichiometric. A value of $\phi = 0$ corresponds to the equilibrium attained when $\Delta\lambda^{\triangleleft} = 0$. When $\phi < 0$, the stored oxygen on the catalyst is less than the stoichiometric equilibrium value and when $\phi > 0$, the stored oxygen is greater than the stoichiometric equilibrium value. In this work, $\mathcal{N}(\phi)$ is parameterized using a quintic polynomial expansion of ϕ.

$$\mathcal{N}(\phi) = a_1\phi + a_2\phi^2 + a_3\phi^3 + a_4\phi^4 + a_5\phi^5. \tag{3}$$

Fig. 2 presents an example of this function based on measured automotive catalyst response data. As ϕ increases from zero, it becomes progressively harder to store oxygen on the catalyst and as ϕ decreases from zero, it becomes progressively harder to remove oxygen from the catalyst. The stored oxygen level does not hit hard saturation/depletion limits, as in limited integrator models, but instead approaches these limits asymptotically while attaining an operating condition that is dependent on the steady-state pre-catalyst air fuel ratio. In this work, we will assume that the model parameters a_1 through a_5 remain constant. In practice, these parameters would have to be adapted to account for temperature dependence and catalyst aging effects.

The post-catalyst, or final tail-pipe, air fuel ratio deviation from stoichiometric $\Delta\lambda^{\triangleright}$ is determined from the oxygen capacity function by the relationship

$$\Delta\lambda^{\triangleright} = \begin{cases} 0, & (\Delta\lambda^{\triangleleft} < 0) \text{ and } (\phi > 0), \\ \mathcal{N}(\phi), & \text{otherwise}, \end{cases} \tag{4}$$

where the pre-catalyst air fuel ratio, $\Delta\lambda^{\triangleleft}$, is denoted using a left-facing triangle and the post-catalyst air fuel ratio, $\Delta\lambda^{\triangleright}$, is denoted using a right-facing triangle. The system is demand limited in the case of rich pre-catalyst exhaust gas, $\Delta\lambda^{\triangleleft} < 0$, and an oxidized catalyst, $\phi > 0$, where stored oxygen is available for reducing the rich exhaust gas, because the oxygen release is limited by the exhaust gas oxygen demand resulting in stoichiometric post-catalyst exhaust, $\Delta\lambda^{\triangleright} = 0$.

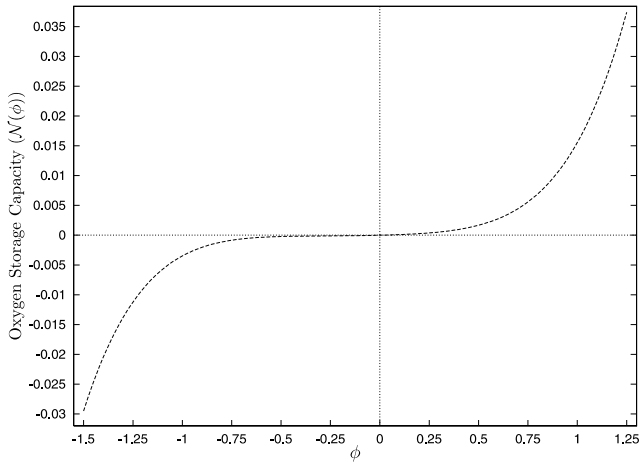

Fig. 2. Normalized oxygen storage capacity $\mathcal{N}(\phi)$.

3.2. Post-catalyst UEGO sensor distortion

The post-catalyst UEGO sensor distortion under rich air fuel ratio operating conditions illustrated in Fig. 1 can be related to the hydrogen generated by catalytic promotion of the water gas shift reaction.

$$CO + H_2O \rightleftharpoons CO_2 + H_2$$

When the reaction proceeds in the forward direction, the ability of hydrogen to diffuse faster than the other gas components results in a sensor output that appears richer than the true value. In the same manner, reduced levels of post-catalyst hydrogen due to a progressive inhibition of the water gas shift reaction result in a sensor output that appears leaner than the true value [5]. The rise toward leaner values of the measured post-catalyst air fuel ratio stoichiometric deviation shown in Fig. 1 is due to this effect. The pre-catalyst sensor dependency on composition can be largely removed by calibration with representative engine-out exhaust. Because the post-catalyst composition varies dynamically according to the reactions taking place, static calibration is insufficient to correct for these errors.

This behavior suggests that the sensor distortion can be used as a measure of the reversible catalyst deactivation effect [6]. If the degree of water gas shift reaction inhibition is assumed proportional to the deactivated fraction of the catalyst surface, ψ, then the apparent post-catalyst air fuel ratio, $\Delta\lambda_a^{\triangleright}$, can be related to the true post-catalyst air fuel ratio, $\Delta\lambda^{\triangleright}$, as follows

$$\Delta\lambda_a^{\triangleright} = \Delta\lambda^{\triangleright} + K_\psi\psi, \tag{5}$$

where the constant K_ψ represents the combined effects of the sensor sensitivity to hydrogen concentration and the inhibition of the water gas shift reaction due to reversible catalyst deactivation. The reversible deactivation model state is determined as follows

$$\dot{\psi} = \dot{m}_f \begin{cases} -K_d(\Delta\lambda^{\triangleright} + \psi), & (\Delta\lambda^{\triangleleft} < 0) \text{ and } (\Delta\lambda^{\triangleright} < 0), \\ -K_r\Delta\lambda^{\triangleleft}, & (\Delta\lambda^{\triangleleft} > 0) \text{ and } (\psi > 0), \\ 0, & \text{otherwise}, \end{cases} \tag{6}$$

where $\Delta\lambda^{\triangleright}$ is the true post-catalyst air fuel ratio determined from the oxygen storage model in Eq. (4) and the sensor distortion of the measured post-catalyst air fuel ratio can be determined from Eq. (5). This model assumes that the rate of deactivation is proportional to the post-catalyst oxygen deficiency, $\Delta\lambda^{\triangleright}$, and the fraction of the surface that is already deactivated, ψ, where K_d is the deactivation constant of proportionality. The

presence of pre-catalyst free oxygen, $\Delta\lambda^{\triangleleft} > 0$, reverses the deactivation process at a rate proportional to the supply of pre-catalyst oxygen until the catalyst is reactivated, $\psi = 0$, where K_r represents the reactivation proportionality constant.

The two states of the combined catalyst model are represented by Eqs. (1) and (6). Fig. 3 presents a comparison between the measured post-catalyst air fuel ratio and the model prediction for the a series of representative step transitions to the pre-catalyst air fuel ratio. As shown in this figure, the deviations at the end of each rich cycle are accounted for in the combined model. In particular, the combined model now characterizes the distortion that occurs in the post-catalyst sensor under rich air fuel ratio engine operation. The close agreement between the predicted and actual measurements, especially during the periods of rich operation, demonstrates that the reversible catalyst deactivation dynamics are well described by this model.

3.3. Pre-catalyst air fuel ratio and fuel system models

The model-based controller in this work will set the target to the engine air fuel ratio controller. The engine air fuel ratio control system will maintain the pre-catalyst exhaust gas at this target through feedback control using the pre-catalyst air fuel ratio sensor. Although there is significant complexity to the air fuel ratio system dynamics due to the effects of fuel puddling, wall wetting, and intake manifold hydrodynamics, a properly functioning air fuel ratio control can essentially eliminate these nonlinear effects on the pre-catalyst air fuel ratio. The closed-loop behavior of the pre-catalyst air fuel ratio can then be approximated by the first order delay-differential equation

$$\tau_\lambda \frac{d\Delta\lambda^{\triangleleft}}{dt} + \Delta\lambda^{\triangleleft} = \Delta\lambda^{*}(t - t_\lambda), \tag{7}$$

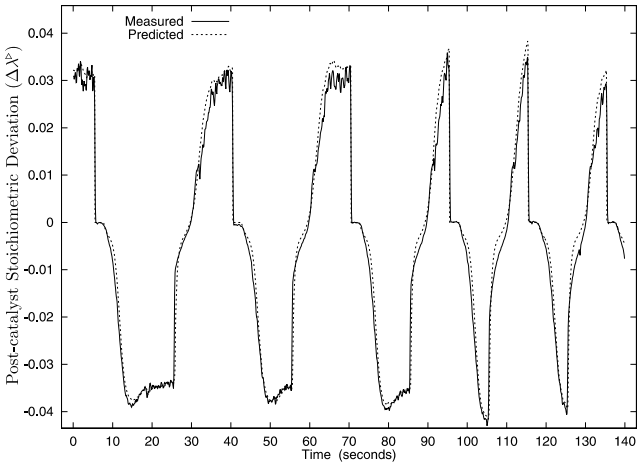

Fig. 3. Post-catalyst air fuel ratio model prediction.

where $\Delta\lambda^*$ is the target air fuel ratio deviation from stoichiometric and t_λ is the time delay.

A feedforward correction to the air fuel ratio target will be made based on engine demand as indicated by the fuel flow commanded by the engine management system. Assuming a first order response between the fuel mass flow rate to the engine and the fuel command, the fuel mass flow rate can be determined as follows

$$\tau_m \frac{d\dot{m}_f}{dt} + \dot{m}_f = \dot{m}_f^{*}, \tag{8}$$

where $\dot{m}_f^*$ is the target fuel command from the engine management system and $\dot{m}_f$ is the fuel mass flow rate to the engine.

3.4. Discrete-time system model

Because a discrete controller will be implemented, the catalyst model presented in Eqs. (1)–(8) is referenced to a nominal fuel mass flow rate and discretized where

$$\tilde{\phi} = \phi/(K_\lambda \dot{m}_f^{\mathrm{ref}}) \tag{9}$$

is the normalized oxygen storage state and $\dot{m}_f^{\mathrm{ref}}$ is the reference fuel flow rate. The discrete model is obtained from integration of the catalyst state model over one controller sample period

$$\tilde{\phi}_{k+1} = \tilde{\phi}_k + \int_{t=k\Delta t}^{(k+1)\Delta t} \rho(\Delta\lambda^{\triangleleft} - \mathcal{N}(\phi))\, dt, \tag{10}$$

where k is the discrete sample period index, Δt is the controller sample period, and $\rho = \dot{m}_f/\dot{m}_f^{\mathrm{ref}}$. This integral can be evaluated by first solving the pre-catalyst air fuel ratio differential equation in Eq. (7) and the fuel mass flow rate differential equation in Eq. (8) at sample period k assuming zero order holds on the engine air fuel ratio target and fuel command in which $\rho_k^* = \dot{m}_{f_k}^*/\dot{m}_f^{\mathrm{ref}}$, and $d_\lambda = t_\lambda/\Delta t$ is the air fuel ratio controller delay in sample periods.

$$\Delta\lambda^{\triangleleft}(t) = \Delta\lambda^{*}_{k-d_\lambda}[1 - e^{-t/\tau_\lambda}] + \Delta\lambda_k^{\triangleleft} e^{-t/\tau_\lambda} \tag{11}$$

$$\rho(t) = \rho_k^{*}[1 - e^{-t/\tau_m}] + \rho_k e^{-t/\tau_m} \tag{12}$$

Substituting these relationships into Eq. (10) and integrating results in the following discrete-time catalyst oxygen storage model

$$\begin{aligned}\tilde{\phi}_{k+1} = \tilde{\phi}_k &+ \alpha\Delta\lambda^{*}_{k-d_\lambda}\rho_k^{*} + \beta\Delta\lambda_k^{\triangleleft}\rho_k^{*} + \gamma\Delta\lambda^{*}_{k-d_\lambda}\rho_k \\ &+ \delta\Delta\lambda_k^{\triangleleft}\rho_k - \epsilon\rho_k^{*} - \zeta\rho_k,\end{aligned} \tag{13}$$

where the constants α–ζ are

$$\alpha = \Delta t - a_\lambda\tau_\lambda - a_m\tau_m + a_{\lambda m}\frac{\tau_\lambda\tau_m}{\tau_\lambda + \tau_m}, \tag{14}$$

$$\beta = a_\lambda\tau_\lambda - a_{\lambda m}\frac{\tau_\lambda\tau_m}{\tau_\lambda + \tau_m}, \tag{15}$$

$$\gamma = a_m\tau_m - a_{\lambda m}\frac{\tau_\lambda\tau_m}{\tau_\lambda + \tau_m}, \tag{16}$$

$$\delta = a_{\lambda m}\frac{\tau_\lambda \tau_m}{\tau_\lambda + \tau_m}, \tag{17}$$

$$\epsilon = (\Delta t + a_m \tau_m)\tilde{\mathcal{N}}(\tilde{\phi}_k), \tag{18}$$

$$\zeta = -a_m \tau_m \tilde{\mathcal{N}}(\tilde{\phi}_k), \tag{19}$$

a_λ, a_m, and $a_{\lambda m}$ are defined aso

$$a_\lambda = \left(1 - \mathrm{e}^{-\frac{\Delta t}{\tau_\lambda}}\right), \quad a_m = \left(1 - \mathrm{e}^{-\frac{\Delta t}{\tau_m}}\right),$$

$$a_{\lambda m} = \left(1 - \mathrm{e}^{-\frac{\Delta t(\tau_\lambda + \tau_m)}{\tau_\lambda \tau_m}}\right)$$

and $\tilde{\mathcal{N}}(\tilde{\phi}_k)$ is the discrete catalyst capacity function.

$$\tilde{\mathcal{N}}(\tilde{\phi}_k) = \sum_{j=1}^{5} a_j (K_\lambda \dot{m}_\mathrm{f}^\mathrm{ref} \tilde{\phi}_k)^j. \tag{20}$$

Utilizing the same procedure for the reversible deactivation model results in the discrete-time model

$$\tilde{\psi}_{k+1} = \tilde{\psi}_k + \begin{cases} -K_\mathrm{d}\left((\Delta t + \zeta)\rho_k^* - \zeta \rho_k\right)(\Delta\lambda_k^\triangleright + \dot{m}_\mathrm{f}^\mathrm{ref}\tilde{\psi}_k), \\ \quad (\Delta\lambda_k^\triangleleft < 0) \text{ and } (\Delta\lambda_k^\triangleright < 0) \\ -K_\mathrm{r}\left(\alpha\Delta\lambda_{k-d_\lambda}^* \rho_k^* + \beta\Delta\lambda_k^\triangleleft \rho_k^* + \gamma\Delta\lambda_{k-d_\lambda}^* \rho_k + \delta\Delta\lambda_k^\triangleleft \rho_k\right), \\ \quad (\Delta\lambda_k^\triangleleft > 0) \text{ and } (\tilde{\psi}_k > 0) \\ 0, \quad \text{otherwise}, \end{cases} \tag{21}$$

where the actual and apparent post-catalyst air fuel ratio discrete model predictions are determined as follows:

$$\Delta\lambda_k^\triangleright = \begin{cases} 0, & (\Delta\lambda_k^\triangleleft < 0) \text{ and } (\tilde{\phi}_k > 0), \\ \tilde{\mathcal{N}}(\tilde{\phi}_k), & \text{otherwise}, \end{cases} \tag{22}$$

$$\Delta\lambda_{a,k}^\triangleright = \Delta\lambda_k^\triangleright + K_\psi \dot{m}_\mathrm{f}^\mathrm{ref}\tilde{\psi}_k.$$

4. Oxygen storage state estimation

Pre- and post-catalyst UEGO sensors are used to estimate the current oxygen storage state of the catalyst. This state estimate can then be used by the model-based controller to determine the future engine air fuel ratio target trajectory to obtain the desired catalyst system performance. A problem with this model-based control strategy is that the desired engine operation results in significant periods of stoichiometric post-catalyst air fuel ratio. The oxygen storage state is then unobservable because changes in the engine exhaust gas have, at least to a first approximation, no effect on the post-catalyst air fuel ratio. Examination of Eq. (4) reveals that the catalyst state for the model presented here cannot be reconstructed from the pre- and post-catalyst air fuel ratio sensors when $\Delta\lambda^\triangleleft < 0$ and $\phi > 0$. Although it is possible to change the operation to provide additional post-catalyst sensor information, this practice would result in increased tail-pipe emissions and could not be applied in a regular fashion. When sensor information is available to estimate the catalyst state, the estimate must then be based on rather noisy air fuel ratio measurements. In this work, a moving horizon least squares estimator analogous to that presented in [7] is constructed to addresses these issues.

The single estimated parameter ω_k is obtained at sample time k from the solution to the following nonlinear least squares problem

$$\begin{aligned} \min_{\omega_k} \quad & \sum_{k-N_\omega}^{k} (\Delta\lambda_{a,k}^\triangleright - \Delta\lambda_{m,k}^\triangleright)^2 + r_\omega\ \omega_k^2 \\ \text{s.t.:} \quad & \tilde{\phi}_{k-N_\omega|k} = \tilde{\phi}_{k-N_\omega|k-1} + \omega_k \\ & \omega_\mathrm{min} \leqslant \omega_k \leqslant \omega_\mathrm{max} \end{aligned} \tag{23}$$

where ω_k is an estimated correction to the oxygen storage state at the beginning of the horizon, N_ω is the horizon length, $\Delta\lambda_{a,k}^\triangleright$ is the model predicted apparent post-catalyst air fuel ratio stoichiometric deviation, $\Delta\lambda_{m,k}^\triangleright$ is the measured post-catalyst air fuel ratio deviation, r_ω is the weighting term on the estimate, and $\tilde{\phi}_{k-N_\omega|k}$ is the corrected initial oxygen state in the horizon. This estimation algorithm is the initial state moving horizon estimator discussed in [8].

The choice of model correction depends on how well it captures the dynamic nature of the true disturbances and how sensitive the model output is to the correction. This estimator is well motivated if the unmodeled disturbances are negligible and the post-catalyst measurement is corrupted by zero mean noise. If the system is unobservable over the estimation horizon, the penalty on the estimated state correction will prevent the estimation algorithm from introducing a large correction that will drive the catalyst model out of demand limited operation. Extended Kalman filtering approaches, such as presented in [9] and [10], do not behave in a similar manner when the model is unobservable. The filter must either be constrained or detuned when the system is unobservable, as discussed in [10], in order to prevent this behavior.

Because a single parameter is estimated by this algorithm, the determination of the sequence $\{\omega_k\}$ can be carried out as a series of one-dimensional optimization or search problems that are not computationally demanding. Provided a feasible sequence is generated by the optimization procedure [12], an approximate solution is available if the computational time limit is reached before convergence. Other corrections, such as a bias to the measured pre-catalyst air fuel ratio stoichiometric deviation or a multiplicative factor to the space velocity, could also be applied to construct the moving horizon estimator but result in poor estimator performance as shown in [11].

We test the moving horizon estimator on the engine operating data presented in Fig. 4. The pre-catalyst air fuel ratio is operated approximately at stoichiometry

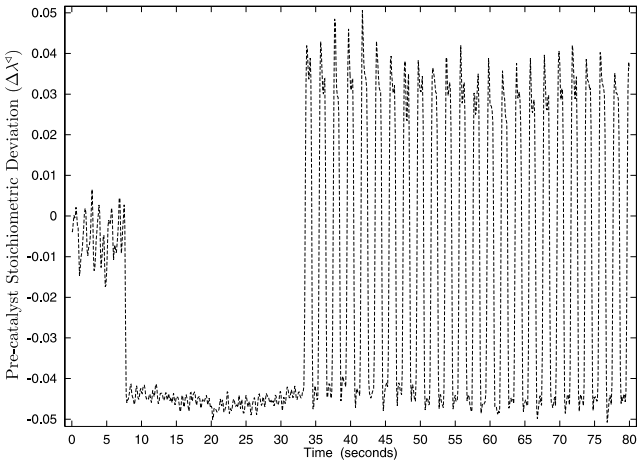

Fig. 4. Example engine operation.

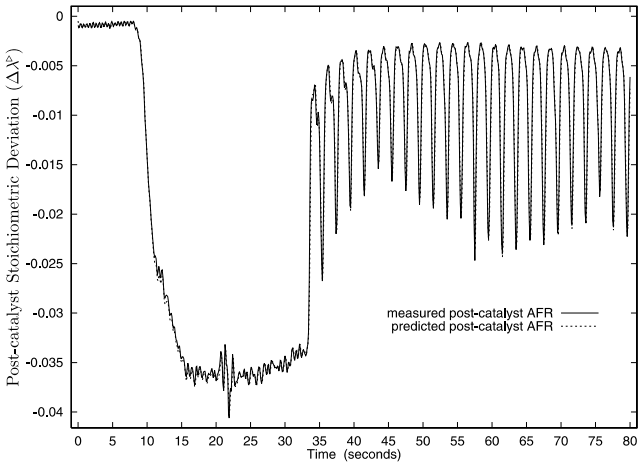

Fig. 6. Post-catalyst estimated air fuel ratio.

for the first 8 s and then operated rich for the next 25 s in order to precondition the catalyst to an oxygen depleted state. After this point, it is cycled between lean and rich operation at a frequency of 1 Hz. When the catalyst oxygen storage level is near depletion or saturation, the magnitude of the gain relating a change in the output $\Delta\lambda^{\triangleright}$ to a change in the catalyst state ϕ is large and the model prediction is generally good as shown in Fig. 3. When the oxygen storage level is closer to its stoichiometric equilibrium level, as in the high frequency portion of the engine operating data in this example, the magnitude of this gain approaches zero and the output is much less sensitive to the catalyst state. Under these conditions, the effects of noise and unmodeled dynamics, when integrated by the model, can result in larger prediction errors. The estimated oxygen storage state $\tilde{\phi}_k$ and the state correction ω_k for the engine operation in Fig. 4 with a sample period of $\Delta t = 0.1$ s and a horizon of $N_\omega = 10$ is presented in Fig. 5 . As shown in this figure, the state corrections are essentially zero for the low frequency engine operation. During the high frequency

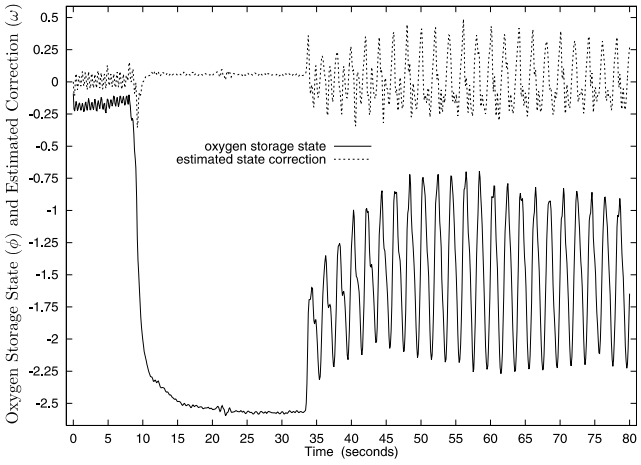

Fig. 5. Estimated oxygen storage state and correction.

operation, larger state corrections are necessary to accurately predict the magnitude of the post-catalyst air fuel ratio oscillations. The estimated post-catalyst air fuel ratio, shown in Fig. 6, is essentially the same as the measured values when these state corrections are applied.

5. Model-based catalyst control strategy

From a control perspective, the post-catalyst air fuel ratio stoichiometric deviation should ideally remain at $\Delta\lambda^{\triangleright} = 0$ to maximize catalyst efficiency and minimize the vehicle tail-pipe emissions. When $\Delta\lambda^{\triangleright} < 0$, there is the possibility of hydrocarbon breakthrough. When $\Delta\lambda^{\triangleright} > 0$, there is the possibility of nitrogen oxide breakthrough. Therefore, the catalyst is typically operated such that the oxygen storage level is always either filling or emptying around the stoichiometric equilibrium storage level. A common practice to achieve this operation is to cycle the pre-catalyst air fuel ratio across stoichiometric at a frequency determined during engine calibration or obtained through relay feedback from a relay type post-catalyst heated exhaust gas oxygen (HEGO) sensor. The output of such sensors switches sharply around stoichiometry resulting in a limit cycle behavior of the catalyst system [1]. A slightly more sophisticated model-based control strategy would aim to maintain the catalyst near the stoichiometric equilibrium state in order to maximize the time required to reach either rich or lean breakthrough conditions when subject to disturbances. Linear model-based control strategies of this type using limited-integrator oxygen storage models have been proposed based on H_∞ [13], linear quadratic regulator [14], and IMC [3] design methods. A nonlinear model predictive control formulation based on this model form is presented in [15]. The strategy adopted in this work allows ϕ to vary dynamically depending on engine demand while preventing post-catalyst break-

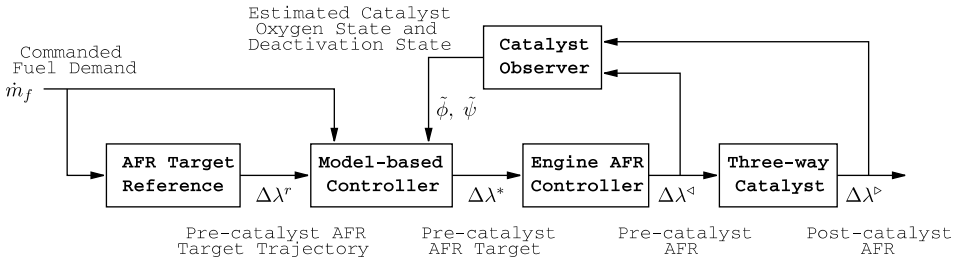

Fig. 7. Model-based controller block diagram.

through as proposed in [16]. A block diagram of this model-based control strategy is presented in Fig. 7. The controller components in this diagram are discussed in the following sections.

5.1. Model-based control algorithm

A nonlinear model predictive control formulation based on the model presented in the present work can be developed as follows

$$\begin{aligned} \min_{\{\Delta\lambda_i^*\}} \quad & \sum_{i=k+d_\lambda}^{k+N} (\Delta\lambda_i^{\triangleleft} - \Delta\lambda_i^r)^2 + r(\Delta\lambda_i^*)^2 + q(\tilde{\phi}_i)^2 \\ \text{s.t.:} \quad & \Delta\lambda^*_{\min} \leqslant \Delta\lambda^*_i \leqslant \Delta\lambda^*_{\max} \\ & \Delta\lambda^{\triangleright}_{\min} \leqslant \Delta\lambda^{\triangleright}_i \leqslant \Delta\lambda^{\triangleright}_{\max} \end{aligned} \tag{24}$$

in which $\Delta\lambda_i^r$ is the pre-catalyst exhaust air fuel ratio reference trajectory based on engine demand, r is the penalty on the pre-catalyst air fuel ratio target deviations from stoichiometric, q is the penalty on the deviation of the oxygen storage state of the catalyst from the equilibrium value of zero, N is the prediction horizon, and $\Delta\lambda^*$ is the pre-catalyst air fuel ratio target sent to the engine AFR controller. The hard constraints in Eq. (24) represent the operational limits for the engine air fuel ratio controller target and the emission limits for the post-catalyst air fuel ratio. Although this control algorithm will dynamically trade off catalyst oxygen storage level for either improved torque or improved fuel economy, it is assumed that $\phi = 0$ is the optimum equilibrium oxygen storage level. The actual optimum equilibrium value of ϕ will depend on the relative oxidation verses reduction rates, the relative probability and magnitude of rich verses lean disturbances, and the relative penalties incurred for rich verses lean post-catalyst breakout.

The application of this model-based controller requires the on-line optimization of the multi-objective performance function proposed in Eq. (24). The direct solution of this optimization problem within the time scale of interest, however, is limited by the computational capability of the engine control module. A weighted Gaussian radial basis function approximation to the optimal solution is presented in [15] to address this computational limitation. Other options include functional parameterization of the future control horizon $\{\Delta\lambda_i^*\}$ to reduce the dimension of the optimization space and multi-rate control approaches in which a fast inner-loop controller, such as a local linear predictive controller, is reset by the nonlinear model predictive controller.

5.2. Air fuel ratio target reference

The pre-catalyst exhaust air fuel ratio reference trajectory, $\Delta\lambda^r$, is determined based on engine demand. As the throttle position is increased, there is an increased demand on the engine. One method to maximize engine performance in this case, is to drive the pre-catalyst air fuel ratio as rich as possible while avoiding catalyst breakout immediately after the throttle position is increased. This action maximizes engine torque early in the demand cycle where it can provide the most benefit. The control system can then reduce the air fuel ratio to allow the catalyst to recover stored oxygen later in the demand cycle. To maximize fuel economy when the throttle position is decreased, the control system could increase the air fuel ratio while avoiding catalyst breakout immediately after the throttle position is decreased. This action minimizes engine fueling at higher engine speeds resulting in reduced fuel consumption during deacceleration. The control system can then make a rich adjustment to the air fuel ratio later in the cycle to prevent lean catalyst breakout. The exact timing and magnitude of these corrections depend on the engine torque characteristics, catalyst capacity, and the trade-off between optimizing engine performance, fuel economy, and vehicle emissions. For example, a very aggressive strategy to optimize engine performance or fuel economy can result in increased emissions because the post-catalyst air fuel ratio will spend more time operating near breakout conditions where the catalyst is more susceptible to disturbances.

The exact characterization of these adjustments for a particular engine system is beyond the scope of this work. However, we note that a lead/lag adjustment to the current air fuel ratio target based on the change in the commanded fuel flow rate provides a simple model that is capable of computing air fuel ratio target reference trajectories with the desired properties. For a change in the commanded fuel flow target at sample

time k, the pre-catalyst air fuel ratio reference can be computed by

$$\Delta\lambda^r_{k+j} = \Lambda(\Delta\lambda^*_k, \Delta\rho^*_k)\exp(-j\Delta t/\sigma) \tag{25}$$

$$\Lambda(\Delta\lambda^*_k, \Delta\rho^*_k) = \begin{cases} \Delta\lambda^*_k - v\Delta\rho^*_k, & (\Delta\lambda^*_k < 0) \text{ and } (\Delta\rho^*_k > 0) \\ \Delta\lambda^*_k - v\Delta\rho^*_k, & (\Delta\lambda^*_k > 0) \text{ and } (\Delta\rho^*_k < 0) \\ -v\Delta\rho^*_k, & (\Delta\lambda^*_k > 0) \text{ and } (\Delta\rho^*_k > 0) \\ -v\Delta\rho^*_k, & (\Delta\lambda^*_k < 0) \text{ and } (\Delta\rho^*_k < 0) \end{cases}$$

where $\Lambda(\Delta\lambda^*_k, \Delta\rho^*_k)$ specifies the instantaneous change in the air fuel ratio target at sample time k, $\Delta\rho^*_k$ is the change in the normalized commanded fuel flow target at sample time k, σ is a tuning parameter that specifies the reference trajectory speed of response, and v is a tuning parameter that specifies the magnitude of the air fuel ratio correction for a change in the normalized engine fuel flow command. In practice, the value of v would be adjusted based on the current engine load and speed.

The reference trajectory is shifted forward at each sample period when the commanded fuel flow target is unchanged and is recomputed from the current pre-catalyst air fuel ratio target when the commanded fuel flow rate changes. The pre-catalyst air fuel ratio approaches stoichiometric at steady state with this adjustment strategy. The catalyst oxygen storage state ϕ is restored to the equilibrium value at steady state through the penalty on the deviation of this state from zero in the model predictive controller objective in Eq. (24).

Fig. 8 presents an example pre-catalyst air fuel ratio target reference trajectory for an increase in the commanded fuel flow target while the current air fuel ratio target is rich. In this case, the reference trajectory further decreases the pre-catalyst air fuel ratio to provide additional engine torque. For this example, $\Delta t = 0.1$ s, $\sigma = 0.75$ s, $v = 0.025$, and the change in the normalized commanded fuel flow rate is $\Delta\rho^* = 0.5$. We note that this tuning provides a performance-aggressive reference trajectory in order to illustrate the intent of the pre-catalyst air fuel ratio target trajectory determination procedure.

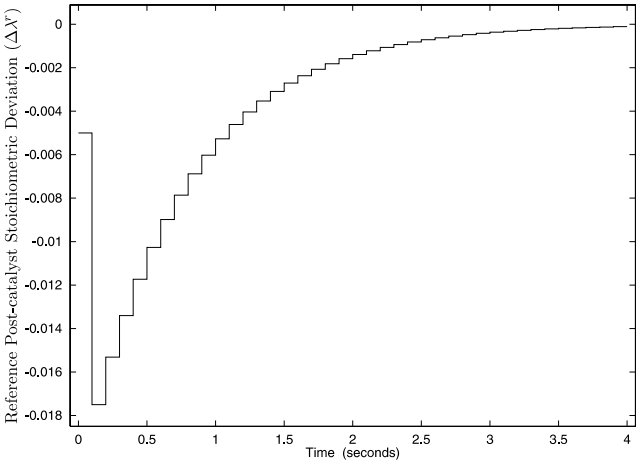

Fig. 8. Pre-catalyst air fuel ratio reference trajectory.

6. Example

An example of the model based controller in this work is presented for an increase in engine demand. In this example, we wish to maximize engine performance by minimizing the pre-catalyst air fuel ratio during the demand cycle. Maximum performance is achieved by setting the pre-catalyst air fuel ratio deviation reference equal to the minimum constraint, $\Delta\lambda^r = \Delta\lambda^*_{\min}$, and not penalizing the pre-catalyst and the post-catalyst air fuel ratio deviations, $q = r = 0$. This choice of tuning maximizes the engine torque subject to the position constraints in Eq. (24). The controller tuning in this example represents an extreme operating condition that would not typically be desired in an engine control system, however, it does illustrate the intent and demonstrate the flexibility of the control algorithm.

Table 1 presents the model parameters used in this example. The catalyst is initially at a steady-state of $\tilde{\phi} = 0$ when a step change from $\rho^* = 1$ to $\rho^* = 1.5$ is made at time $t = 0$. The pre-catalyst air fuel ratio target position constraints are $\Delta\lambda^*_{\min} = -0.025$ and $\Delta\lambda^*_{\max} = 0.025$. The post-catalyst air fuel ratio position constraints which represent the catalyst breakout limits are $\Delta\lambda^{\triangleright}_{\min} = -0.001$ and $\Delta\lambda^{\triangleright}_{\max} = 0.001$.

As shown in Fig. 9, the controller immediately saturates the pre-catalyst air fuel ratio deviation target at $\Delta\lambda^* = -0.025$ to maximize the attainable engine torque early in the demand cycle. The result is a depletion of the stored oxygen on the catalyst and a decrease in the post-catalyst air fuel ratio. After approximately 3.5 s, the controller brings the air fuel ratio deviation target back close to stoichiometric, $\Delta\lambda^* = 0$, to prevent the post-catalyst air fuel ratio from violating the minimum breakthrough constraint. The controller then slowly brings the air fuel ratio deviation target down to the minimum post-catalyst constraint value and holds at this value so that the steady-state post-catalyst air fuel ratio does not violate the minimum constraint. The engine operates at the post-catalyst air fuel ratio minimum constraint from approximately 5 s into the demand cycle. Because of the rich bias in the catalyst operation, the apparent post-catalyst air fuel ratio begins to show a lean bias sensor dis-

Table 1
Model parameters

Variable	Value
Δt	0.1 s
τ_λ	0.5 s
d_λ	2
τ_m	1 s

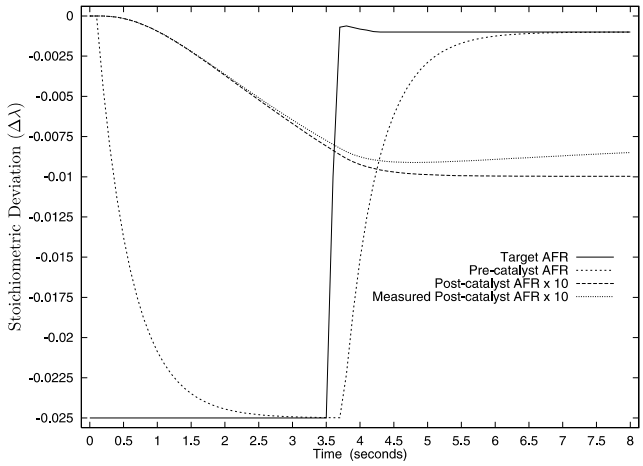

Fig. 9. Air fuel ratio controller performance.

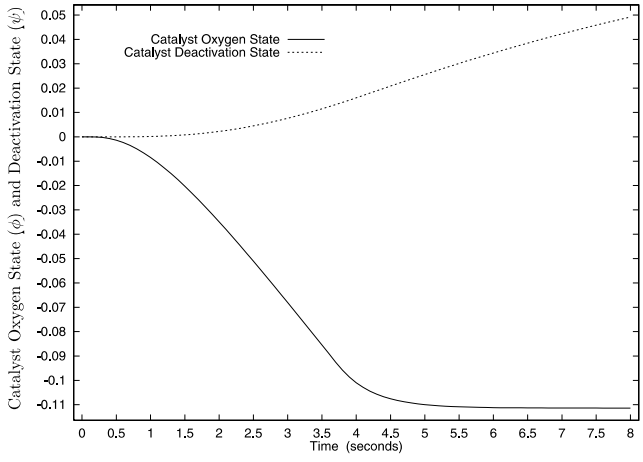

Fig. 10. Oxygen and deactivation state performance.

tortion after 2.5 s into the demand cycle. We note that control based on the post-catalyst UEGO measurement would result in post-catalyst rich breakthrough because of this distortion. Fig. 10 shows the oxygen storage and catalyst deactivation states for the engine operation in this example.

7. Conclusions

The nonlinear model-based controller presented in this work minimizes vehicle emissions while optimizing engine performance and fuel economy during transient engine demand. Engine performance and fuel economy are optimized during transient operation by taking advantage of the oxygen storage capability of the catalyst that allows deviation from stoichiometric operation for short periods of time without post-catalyst emissions. Feedback is provided by a moving horizon estimation scheme for the oxygen storage state that minimizes the post-catalyst air fuel ratio squared prediction error over a past prediction horizon by the selection of a single state correction term. Future work includes adapting the model for catalyst temperature dependence and addressing the computational requirements of the algorithm to allow real-time implementation.

Acknowledgements

Support for this work from the National Science Foundation under Grant CTS-0215920, Ford Motor Company, Johnson Matthey, and ExxonMobil is gratefully acknowledged.

References

[1] P. Eastwood, Exhaust Gas Aftertreatment, Research Studies Press, Baldock, England, 2000.
[2] E. Brant, Y. Wang, J. Grizzle, Dynamic modeling of a three-way catalyst for SI engine exhaust emission control, IEEE Trans. Contr. Syst. Tech. 8 (2000) 767–776.
[3] M. Balenovic, A. Backx, J. Hoebink, On a model-based control of a three-way catalytic converter, SAE Paper 2001-01-0937, SAE World Congress, 2001.
[4] J.C. Peyton Jones, R.A. Jackson, J. Roberts, P. Bernard, A simplified model for the dynamics of a three-way catalytic converter, SAE Paper 2000-01-0652, SAE World Congress, 2000.
[5] J.C. Peyton Jones, R.A. Jackson, Potential and pitfalls in the use of dual EGO sensors for three-way catalyst monitoring and control, Proc. Inst. Mech. Eng. D 217 (2003) 475–488.
[6] J.C. Peyton Jones, Modeling combined oxygen storage and reversible deactivation dynamics for improved emissions predictions, SAE Paper 2003-01-0999, SAE World Congress, 2003.
[7] H. Michalska, D. Mayne, Moving horizon observers and observer-based control, IEEE Trans. Automat. Contr. 40 (1995) 995–1006.
[8] K.R. Muske, T.F. Edgar, Nonlinear state estimation, in: Nonlinear Process Control, Prentice-Hall, Englewood Cliffs, NJ, 1997.
[9] M. Balenovic, J. Edwards, T. Backx, Vehicle application of model-based catalyst control, in: Proceedings of the 1st IFAC Symposium on on Advances in Automotive Control (2004) pp. 351–356.
[10] G. Fiengo, J.A. Cook, J.W. Grizzle, Fore-Aft oxygen storage control, in: Proceedings of the 2002 American Control Conference (2002) pp. 1401–1406.
[11] K.R. Muske, J.C. Peyton Jones, Estimating the oxygen storage level of a three-way automotive catalyst, in: Proceedings of the 2004 American Control Conference (2004) pp. 4060–4065.
[12] J. Nocedal, S.J. Wright, Numerical Optimization, Springer-Verlag, New York, 1999.
[13] E. Shafai, C. Roduner, H. Geering, Indirect adaptive control of a three-way catalyst, SAE Paper 961038, SAE World Congress (1996).
[14] A. Ohata, M. Ohasi, M. Nasu, T. Inoue, Model based air fuel ratio control for reducing exhaust gas emmissions, SAE Paper 950075, SAE World Congress (1995).
[15] M. Balenovic, T. Backx, T. de Bie, Development of a model-based controller for a three-way catalytic converter. SAE Paper 2002-01-0475, SAE World Congress (2002).
[16] K.R. Muske, J.C. Peyton Jones, Feedforward/Feedback air fuel ratio control for an automotive catalyst, in: Proceedings of the 2003 American Control Conference (2003) pp. 1386–1391.